Suppressing mechanical dissipation of diamagnetically levitated oscillator via engineering conductive geometry

Han Xie [1,*] Yanan Li [1,*] Rui Li,[2,3,4,*] Yinchun Leng [1] Yiming Chen,[1] Lei Wang,[1] Dingjiang Long [1] Xiang Bian [1] Chang-Kui Duan,[2,3,4] Peiran Yin [1,†] Pu Huang [1] and Jiangfeng Du[2,3,4,‡]

[1]*National Laboratory of Solid State Microstructures and Department of Physics, Nanjing University, Nanjing 210093, China*
[2]*Hefei National Laboratory for Physical Sciences at the Microscale and Department of Modern Physics,
University of Science and Technology of China, Hefei 230026, China*
[3]*CAS Key Laboratory of Microscale Magnetic Resonance, University of Science and Technology of China, Hefei 230026, China*
[4]*Synergetic Innovation Center of Quantum Information and Quantum Physics,
University of Science and Technology of China, Hefei 230026, China*

Diamagnetically levitated oscillators of millimeter and submillimeter size are emerging ultrasensitive sensors for gravitylike force and acceleration measurements. However, improving the levitation capability while keeping mechanical dissipation low remains an open challenge. Here, we propose and experimentally demonstrate an engineering conductive geometry scheme to efficiently reduce the mechanical dissipation of a diamagnetically levitated oscillator made of pyrolytic graphite. We show that with a specially designed conductive geometry, the eddy current damping is reduced, and the reduction factor increases as the engraving pattern being denser. Under high vacuum and room temperature, eddy current damping is the dominant contribution to mechanical dissipation, and we reduce it by a factor of 50 in the experiment. Our work opens up a new way to achieve diamagnetically levitated oscillator with ultralow mechanical dissipation and strong levitation capability, a candidate platform for studying a broad range of fundamental physics.

I. INTRODUCTION

Levitated mechanical oscillators in high vacuum have been emerging to be a promising system extremely isolated from the environment [1]. With ultralow dissipation [2–4], the oscillator has huge advantages in sensing weak signals, for example, the inertia sensing [5–9], single spin detection [10–13], thermometry [14,15], magnetometry [16,17], and tests of wave-function collapse models [18–21]. Recently, the diamagnetically levitated oscillators of millimeter and submillimeter size have been demonstrated to be ultrasensitive for near-surface force detection [22–24] and gravitylike force sensing [25–27], which is of great interest for test of new physics [28–36].

In the measurement of forces proportional to the amount of atoms in a diamagnetically levitated oscillator, acceleration sensitivity is crucial. The acceleration sensitivity of the oscillator is limited by the thermal noise:

$$S_{aa}(\omega_0) = \frac{4\gamma k_{\mathrm{B}}T}{m}. \tag{1}$$

Here, γ is the mechanical dissipation, k_{B} is the Boltzmann constant, T is the temperature, and m is the mass of oscillator. At room temperature, the ratio γ/m needs be reduced to improve the sensitivity. Besides, the oscillator should be well suited for the sophisticated structure design to adapt to specific weak signal sensing. Addressing these issues simultaneously is an open challenge: for a diamagnetically levitated oscillator with mass up to 10 mg, strong levitation capability is necessary due to the scaling law of the magnetic field [37,38]; and the dissipation path of such an oscillator of this large size needs to be well-controlled to reduce it mechanical dissipation [12]. Pyrolytic graphite is a strong diamagnetic material that is able to provide sufficient levitation force to counteract the gravity. However, because of eddy currents, the mechanical dissipation of pyrolytic graphite is quite large, resulting in poor acceleration sensitivity.

In this paper, we propose and experimentally demonstrate an engineering conductive geometry scheme to efficiently reduce the mechanical dissipation of the diamagnetically levitated oscillator made of pyrolytic graphite, which is at millimeter scale. Using a specially designed conductive geometry based on theoretical design and numerical simulation, we show that the mechanical dissipation can be significantly reduced and the reduction factor increases as the engraving pattern being denser. For a diamagnetically levitated pyrolytic

---

*These authors contributed equally to this paper and are joint first authors.
†ypr@nju.edu.cn
‡djf@ustc.edu.cn

graphite oscillator, a reduction factor of 50 is achieved in the experiment, in agreement with the theory. The results demonstrated in this work pave the way for establishing a platform of diamagnetically levitated oscillator with ultralow mechanical dissipation and strong levitation capability that can be applied to study a broad range of fundamental physics.

II. THEORETICAL MODEL

The mechanical dissipation γ of diamagnetically levitated oscillators made of pyrolytic graphite is composed of two parts: the air dissipation γ_{air} and the eddy current dissipation γ_{ec}. Air dissipation γ_{air} varies with pressure, and in a high vacuum of 10^{-4} mbar, the contribution of air dissipation is small. The dissipation γ_{ec} comes from the eddy currents created in conductors when the oscillator is moving in a magnetic field, and does not vary with pressure. For a pyrolytic graphite oscillator moving at a velocity $\dot{z}$ in a static magnetic field of **B** in high vacuum, the mechanical dissipation γ is dominated by the eddy current dissipation γ_{ec}. The dissipation term of an oscillator comes from the dissipation force $\boldsymbol{F}_d$, which can be expressed as

$$\boldsymbol{F}_d = -m\gamma\dot{z}. \tag{2}$$

Here, the negative sign means the direction of the dissipation force $\boldsymbol{F}_d$ is opposite to the direction of the velocity $\dot{z}$. In our system, the dissipation force $\boldsymbol{F}_d$ of eddy current is the Lorentz force, which can be expressed as $\boldsymbol{F}_d = \boldsymbol{J} \times \boldsymbol{B}$. If we only consider the velocity $\dot{z}$ along z direction, the eddy current density $\boldsymbol{J}$ can be expressed as $\boldsymbol{J} = -\sigma(\dot{z} \times \boldsymbol{B})$, where σ is the conductivity. We can calculate the eddy current dissipation γ_{ec} in the oscillator by

$$\gamma_{\text{ec}} = \frac{\sigma}{m} \int_V ((B_y \, \boldsymbol{i} - B_x \, \boldsymbol{j}) \times \boldsymbol{B}) \cdot \boldsymbol{k} \, dV, \tag{3}$$

where the $\boldsymbol{i}$, $\boldsymbol{j}$ and $\boldsymbol{k}$ represent the unit vectors along the x, y, and z directions, respectively, and V is the volume of the pyrolytic graphite flake.

To clearly demonstrate the physical principle, pyrolytic graphite flakes without and with engraving pattern are placed in a static magnetic field as shown in Figs. 1(a) and 1(b), respectively. For an unprocessed square pyrolytic graphite flake without the engraving pattern shown in Fig. 1(a), the eddy current loops are approximately a series of concentric square loops around the center of the flake, as indicated by the red arrows. While for a piece of processed pyrolytic graphite flake with engraving pattern shown in Fig. 1(b), the eddy current loops are separated into a series of small loops along the pattern slits. It is what we call the engineering conductive geometry. The pyrolytic graphite flake is engraved through by the designed slits, and the effective resistance for eddy current loops increases. As the eddy current is smaller, the dissipation force $\boldsymbol{F}_d$ decreases, and hence the eddy current dissipation γ_{ec} is suppressed. To reduce the eddy current dissipation γ_{ec} more effectively, we have to carefully design the conductive geometry for the specific diamagnetically levitated oscillators based on numerical simulation. We designed and simulated several different engineering conductive geometry schemes. To maintain the comparability of these schemes, we keep several parameters the same in these schemes: the oscillators
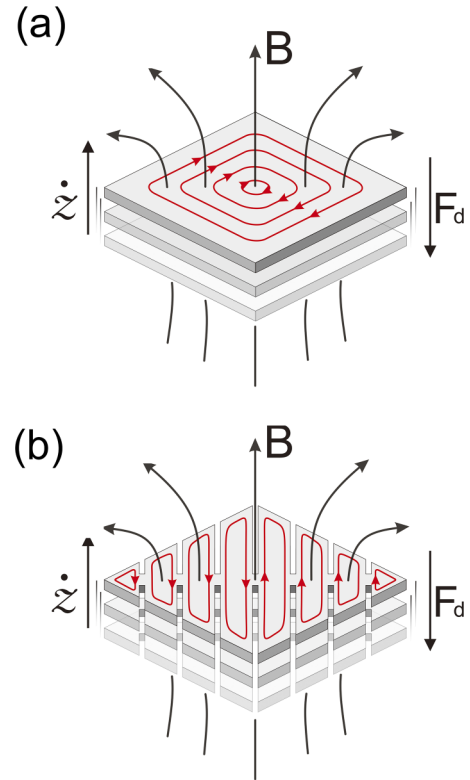

FIG. 1. Eddy currents in pyrolytic graphite oscillators moving in a static magnetic field. The red arrows represent the eddy current loops in an oscillator moving in the z direction with a velocity of $\dot{z}$. The dissipation force caused by the eddy current is $\boldsymbol{F}_d$. (a) The oscillator is made of square pyrolytic graphite flake without engraving pattern, the eddy current loops are approximately a series of concentric square loops around the center of the flake. (b) The oscillator is made of flake with engraving pattern, whose eddy current loops are separated into a series of small loops along the pattern slits.

have the same original size, the engraving width of the slits is set as 10 μm and the length of the remaining part after engraving is 0.5 mm.

Here are some parameters used in the simulation. The pyrolytic graphite has a density of 2.2 g/cm³, the values of conductivity σ along x, y, and z directions are 3.3×10^5 S/m, 3.3×10^5 and 3.3×10^2 S/m, respectively [39]. Its anisotropic magnetic susceptibility χ_V along x, y, z directions are -8×10^{-5}, -8×10^{-5}, and -9×10^{-4}, respectively, the values are measured by a Superconducting Quantum Interference Device. The pyrolytic graphite oscillator, with a size of $5 \times 5 \times 0.2$ mm, moves harmonically in z direction on the top of a magnetogravitational trap. This trap was used in our previous experiment to provide a stable bound in $x - y$ plane [40]: Four $5 \times 5 \times 5$ mm magnets with saturation magnetization 1 T are arranged in a 2×2 matrix. The polarization is along the z axis, and the two magnets in the diagonal position are polarized in the same direction, while the magnets in the adjacent locations are polarized in the opposite direction. This configuration can efficiently levitate pyrolytic graphite flake by creating a steady trap in the top central portion of the magnets. Measured from experiment, the pyrolytic graphite oscillator's levitation height is 0.75 mm.
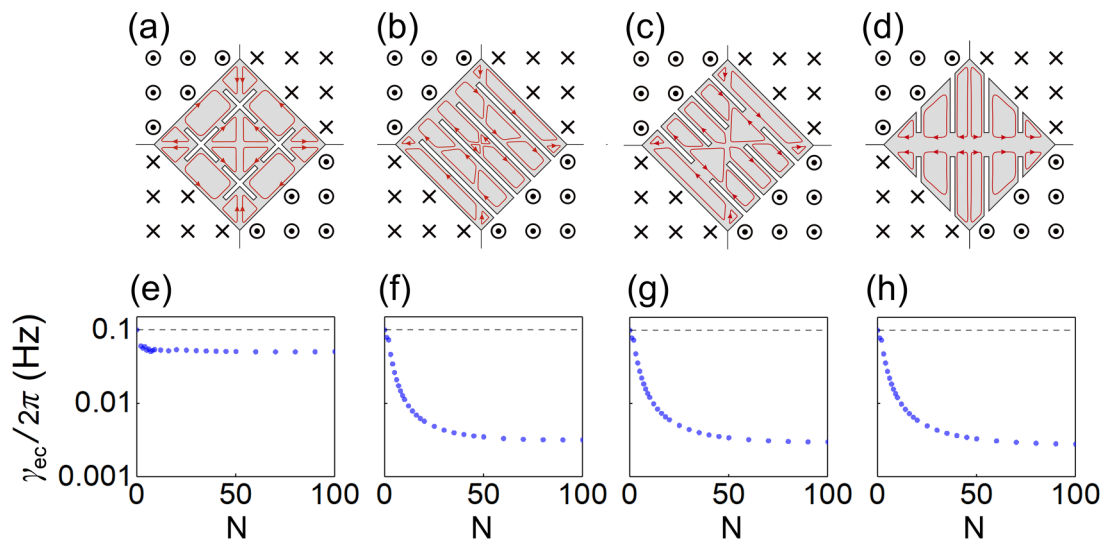
FIG. 2. The eddy current dissipation $\gamma_{ec}/2\pi$ of different engineering conductive geometry schemes with the change of number of slits N obtained by numerical simulation. [(a)–(d)] The magnetic field direction is perpendicular to the paper, the circle represents the magnetic field outward, and the cross represents the magnetic field inward. Here, the number of slits is $N = 4$, and the red arrows represent the directions of eddy current in different schemes when the oscillator moving along z direction, and the information of strength of the current density is omitted. [(e)–(h)] The blue points is the eddy current dissipation $\gamma_{ec}/2\pi$ of the corresponding scheme, and the gray dashed line is the eddy current dissipation $\gamma_{ec}/2\pi$ when $N = 0$, which is 0.1 Hz. The simulation results find that engineering conductive geometry schemes (d) has the lowest dissipation $\gamma_{ec}/2\pi = 2.8$ mHz when $N = 100$.

Figure 2 plots the simulation results of the eddy current dissipation γ_{ec} with different engineering conductive geometry schemes. In Figs. 2(a)–2(d), the static magnetic field direction is perpendicular to the paper direction, the circle represents the magnetic field lines outward the paper, and the cross represents the lines inward the paper. The red arrows indicate the eddy current loops in oscillators, here the number of slits is $N = 4$. The corresponding numerical results of the eddy current dissipation are shown in Figs. 2(e)–2(h). The grey dashed line in the figure indicate the dissipation of unprocessed pyrolytic graphite flake, which is $\gamma_{ec}/2\pi = 0.1$ Hz. For the case with cross-shaped slits shown in Fig. 2(a), the change of the dissipation is not obvious with the increase of N. The reason is that, some eddy currents can travel between the cross-shaped slits, and these eddy current loops will increase as N increases. In the scheme Fig. 2(a), the final dissipation can only reach $\gamma_{ec}/2\pi = 0.05$ Hz. By engraving the graphite into independent strips, we designed another comb-shaped structure in Fig. 2(b), this conductive geometry can prevent the eddy current loops from traveling between each strip. We found that the decline of dissipation is not infinite, it would gradually saturate as N reaches 50, and achieves a minimum dissipation of 3.2 mHz at $N = 100$. The scheme Fig. 2(b) will also sacrifice part of oscillator's mechanical strength due to the overly long engraving slits. And the center of mass of the oscillator is translated away from the center of the square, which will make the oscillator prefer rotating other than translating. Therefore we used the two-side comb-shaped engraving process in Figs. 2(c) and 2(d) as the optimization of scheme Fig. 2(b). The symmetrical designed pattern can maintain the center of mass and ensure sufficient mechanical strength. The direction of the slits is along the side direction in the scheme Fig. 2(c), and along the diagonal direction in the

scheme Fig. 2(d). The corresponding mechanical dissipation are $\gamma_{ec}/2\pi = 3.0$ and 2.8 mHz, respectively.

Through theoretical design and numerical simulation, the engineering conductive geometry scheme can actually reduce the eddy current dissipation γ_{ec} of the pyrolytic graphite oscillator. The lowest dissipation we got so far is in scheme Fig. 2(d) with $\gamma_{ec}/2\pi = 2.8$ mHz. Therefore we experimentally verify the optimization of the eddy current dissipation of the pyrolytic graphite oscillator with scheme Fig. 2(d). There could be better designed schemes waiting to be proposed.

III. EXPERIMENTAL SYSTEM

We tested our scheme using the diamagnetically levitated oscillator made of pyrolytic graphite in high vacuum of 10^{-4} mbar at room temperature. The engineering conductive geometry was achieved by the laser engraving on the pyrolytic graphite flake of size $5 \times 5 \times 0.5$ mm^3. The photo of a square pyrolytic graphite flake without engraving pattern is shown in Fig. 3(a) and the photo of a piece of typical engraved pyrolytic graphite flake with number of slits $N = 20$ is shown in Fig. 3(b). In our experiment, we made oscillators of different numbers of slits, $N = 5, 10, 15, 20$, and 50. The engraving width of slits of the oscillators with $N = 5, 10, 15$, and 20 is 0.1 mm. When $N = 50$, due to the size limitation of the pyrolytic graphite flake, the engraving width is 0.04 mm. It is worth mentioning that after laser engraving, the oscillators with different N have different masses, we polished them in the z direction to ensure that their masses are the same to compare their values of mechanical dissipation γ directly. An oscillator with measurement part is shown in Fig. 3(c). A glass rod is attached onto the center of pyrolytic graphite flake vertically, and a copper wire is glued on the rod
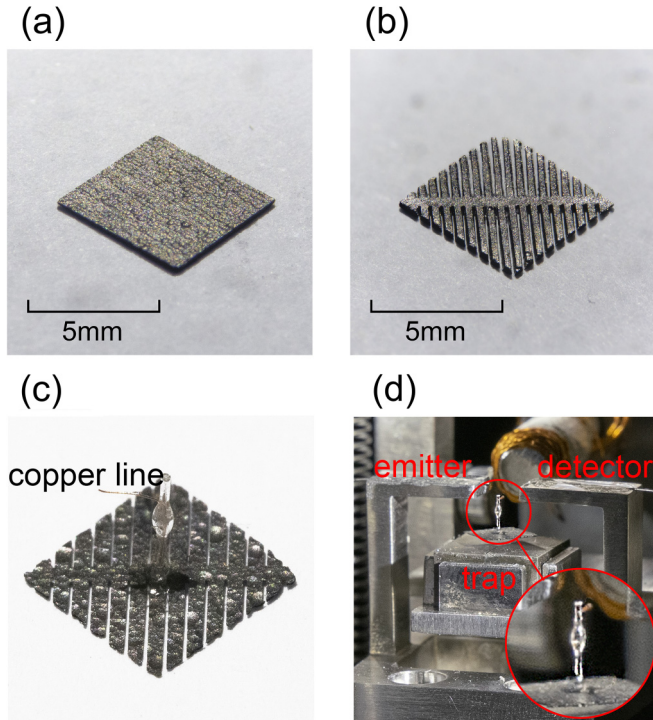
FIG. 3. Photos of the oscillators made of pyrolytic graphite flakes and the experiment system. (a), (b) Photos of unprocessed and processed pyrolytic graphite flakes. (a) The square pyrolytic graphite flake without engraving pattern. (b) Processed pyrolytic graphite flakes with engraving pattern, the number of slits is $N = 20$, the engraving width of the slits is 0.1 mm. (c) The photo of pyrolytic graphite oscillator with measurement part: A glass rod stands on the center of the pyrolytic graphite flake with a horizontal thin copper wire for optical motion detection. Both the glass rod and the copper wire are fixed by UV glue. (d) The experiment system: The oscillator is loaded in the magnetogravitational trap. A 1550-nm laser with the power of the order of μW is applied to fiber on the left as an emitter, while a photodiode is connected to the fiber on the right side as a detector. The laser is scattered by the thin copper wire and is finally received by the detector. The glass rod is enlarged for easy viewing.

horizontally for the optical motion detection. Both the glass rod and the copper wire are fixed by UV glue, and their masses are much smaller than that of the pyrolytic graphite flake, which can minimize the dissipation caused by the measurement part.

The experimental system was positioned on the air flotation platform to isolate the vibration from the ground. As shown in Fig. 3(d), in the vacuum chamber, there are the magnetogravitational trap and the laser detection system. The trap was placed in a specially designed two-stage vibration isolation system to isolate the strong vibration from the pump and other instruments. The detection light path was located approximately 5 mm above the trap. A 1550-nm laser was applied to the fiber on the left as the emitter, while a photodiode was connected to the fiber on the right side as the detector. The magnetogravitational trap was fixed on a motorized positioner. Its position can be adjusted three-dimensionally, so that the position of the oscillator can be adjusted to make sure that the laser can be scattered by the thin copper wire and finally

be received by the detector. The intensity of the scattered light, corresponding to the real-time displacement of the oscillator, was measured by the photodiode. Then the signal was amplified and recorded for further procedure. After loading the oscillator into the trap and adjusting it to a suitable position for motion detection, the circuits of the positioner were removed to avoid unnecessary vibration disturbance. There were 20 turns of copper wires wrapped around an iron core as an excitation coil to generate magnetic driving force, and it was mechanically attached to the first-stage vibration isolation at a distance of 1 cm from the oscillator. Pressure gauges and thermometers were also installed inside the chamber to monitor changes in pressure and temperature in real time.

IV. EXPERIMENT DESCRIPTION AND RESULTS

The method to measure the mechanical dissipation in our experiment is recording the displacement amplitude of pyrolytic graphite oscillator during the total process of free decaying. The free decaying of the oscillator is described by

$$X(t)^2 = X(0)^2 \exp(-\gamma t). \tag{4}$$

The free decaying of $X(t)^2$ is measured by exciting the oscillator to initial displacement amplitude $X(0)$ using an excitation coil. The square of the amplitude $X(0)^2$ decays by a factor of more than 1000 in the measurement. Then the mechanical dissipation γ is obtained by fitting the measured data to the time evolution equation $X(t)^2 = X(0)^2 \exp(-\gamma t)$. In our experiment, the $X(t)^2/X(0)^2$ can be obtained from the power spectral density (PSD) of the oscillator's displacement.

The experiment measurement was carried out in high vacuum at room temperature. The masses of oscillators were 7.9 ± 0.3 mg. In the atmospheric pressure environment, we used a loudspeaker to actuate the whole magnet setup and determined the approximate frequencies of all the oscillator's motion modes. Then in vacuum, we swept the driving force by the excitation coil to determine the accurate frequencies of modes: in x, y, and z axes, the translational frequencies were 7.5, 8.8 and 23.5 Hz, and the rotating frequencies were 16.9, 18.1, and 12.8 Hz, respectively. Among these motion modes, the frequency of z direction translation is the highest. In practice, we choose to study the mechanical dissipation of the translational motion mode along z direction.

Firstly, we used an unprocessed oscillator and a processed oscillator with number of slits $N = 50$ to compare their energy damping time $\tau = 1/\gamma$ in different pressures in the range of 2×10^{-4} mbar to 1×10^{-2} mbar at the same temperature. We repeated the measurement 10 times at each pressure to get the averaged damping time and its standard deviation. Figure 4(a) shows that the unprocessed pyrolytic graphite oscillator's average damping time is 1.3 ± 0.2 s. The corresponding dissipation $\gamma/2\pi = 0.125$ Hz. The fitted curve shows that most of the dissipation is contributed by eddy current dissipation, because its damping time hardly changes with the change of pressure. And the eddy current dissipation is very high. Figure 4(b) shows the damping time of the pyrolytic graphite oscillator after processing with $N = 50$. Its damping time will increase with the decrease of pressure, because the eddy
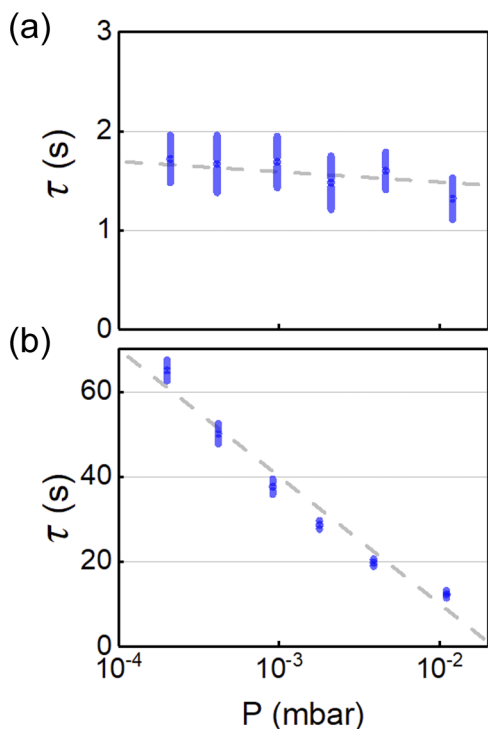
FIG. 4. The damping time τ of unprocessed pyrolytic graphite oscillator and processed oscillator with $N = 50$ in the pressure range of 2×10^{-4} to 1×10^{-2} mbar. (a) The damping time τ of the unprocessed pyrolytic graphite oscillator nearly constant around 1.3 ± 0.2 s. The eddy current dissipation is huge at this time. (b) The damping time τ of the processed oscillator with $N = 50$ will increase with the decrease of pressure. The damping time τ measured under 2×10^{-4} mbar can reach 65 ± 2 s. Taking into consideration that there is still contribution from air dissipation, the eddy current dissipation has been suppressed more than 50 times.

FIG. 5. Experimentally measured free dacaying curve and mechanical dissipation $\gamma/2\pi$. (a) The free dacay curve at room temperature in the pressure of 2×10^{-4} mbar, the mass of oscillators is 7.9 ± 0.3 mg. The solid line represents the measured dacay curve, and the dashed line represents the simulated results, corresponds to $N = 0$ (purple), 5 (black), 10 (blue), 15 (red), 20 (magenta), and 50 (green). The damping time τ of the oscillator at $N = 50$ is increased by a factor of 50 compared to that of $N = 0$. (b) The mechanical dissipation $\gamma/2\pi$ changes with the number of slits N, the blue solid line is the measured $\gamma/2\pi$, and the gray dashed line is the simulated results.

current is significantly reduced. The damping time measured under 2×10^{-4} mbar can reach 65 ± 2 s. Taking into consideration that there is still contribution from air dissipation, the eddy current dissipation has been suppressed more than 50 times.

Then we measured the mechanical dissipation γ of oscillators with different number of slits N at room temperature in a pressure of 2×10^{-4} mbar. For the convenience of comparison, here we made oscillators with different N but the same mass of 7.9 ± 0.3 mg. Figure 5(a) is the normalized free decaying curves $X(t)^2/X(0)^2$ versus time for the z-mode of resonant frequency 23.5 Hz. The solid line represents the measured curves, and the dashed line represents the numerical results from simulated eddy current dissipation, corresponding to $N = 0$(purple), 5 (black), 10 (blue), 15 (red), 20 (magenta), and 50 (green). We can see that the damping time becomes longer as N increases. According to the curves, we get the damping time τ and mechanical dissipation γ of each oscillator, as plotted in Fig. 5(b). The blue solid line is the measured $\gamma/2\pi$, and the gray dashed line is the simulated γ. The damping time τ of the oscillator made of pyrolytic graphite without engraving pattern is only 1.3 s, corresponding to the mechanical dissipation $\gamma/2\pi = 0.12$ Hz. When the number of slits is $N = 50$, the damping time τ can
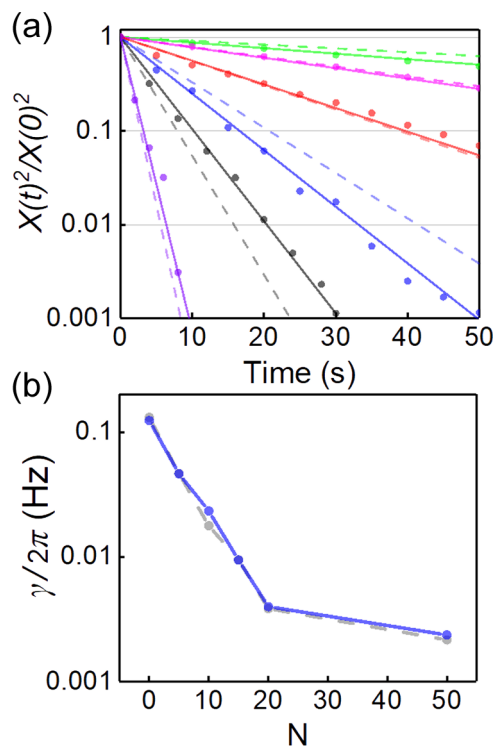
reaches 67 s, corresponding to the mechanical dissipation $\gamma/2\pi = 2.4$ mHz. The damping time increases by a factor of 50 times. It demonstrates that our engineering conductive geometry scheme can effectively reduce the mechanical dissipation γ through preventing the formation of eddy currents. The possible reasons for the small inconsistencies between experiment and numerical results are the following: dense engraving leads to a decrease in mechanical strength and laser engraving fails to break down all the gaps.

With the above method, the oscillator's acceleration sensitivity can be improved from its initial value of 3.5×10^{-9} g/$\sqrt{\text{Hz}}$ to 5.6×10^{-10} g/$\sqrt{\text{Hz}}$. It can be even higher with the growth of pyrolytic graphite oscillator's mass. On magnets with a size of $20\times20\times20$ mm^3, we simulated with pyrolytic graphite oscillators of size $L\times L\times0.2$ mm^3 to compute their γ and acceleration sensitivity. By increasing the length L of the oscillator in x and y direction, and keeping the thickness 0.2 mm, we obtain its mass as a function of the square of the length L^2. The engraving width and the distance between the slits stays constant, the number of slits N increases with the growth of length L. The results of the simulation are displayed in Fig. 6. The oscillator used in our experiment
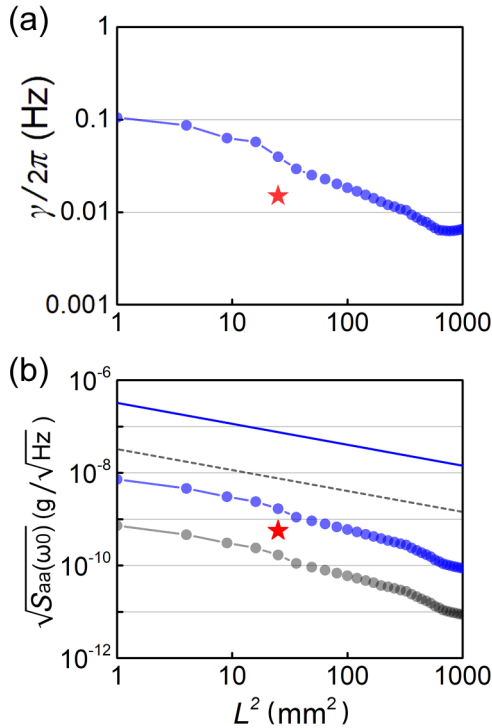
FIG. 6. The theoretical mechanical dissipation $\gamma/2\pi$ and acceleration sensitivity with the change of square of the length L^2. The red stars in (a) and (b) represent the value of the oscillator with $N = 50$ used in our experiment.(a) The blue curve represents the $\gamma/2\pi$ with different L^2, which decreases as the L^2 increases but starts to increase when the L^2 reaches 900 mm^2. The reason is that as the size of the pyrolytic graphite grows to be comparable to the size of the trap, the levitation height decreases.(b)The blue solid line and the black dashed line represent the acceleration sensitivity of the pyrolytic graphite oscillator without engraving pattern at room (298 K) and low (3 K) temperatures, respectively. The blue and black dots represent the acceleration sensitivity of the oscillator with engraving pattern at room temperature and low temperature, respectively. When the oscillator's length reaches 34 mm, the mass is 200 mg and the acceleration sensitivity can reach $\sim 10^{-11}$g/$\sqrt{\text{Hz}}$ at room temperature and $\sim 10^{-12}$g/$\sqrt{\text{Hz}}$ at low temperature.

is represented by the red star in the picture. As shown in Fig. 6(a), as the length of pyrolytic graphite oscillator increases, the γ gradually decreases first but starts to increase when the length reaches 900 mm^2. The reason is that, as the length L increases, the size of the pyrolytic graphite grows to be comparable to the size of the trap, and as a result, the levitation height decreases. In Fig. 6(b), the blue solid line and the black dashed line represent the acceleration sensitivity of the unprocessed pyrolytic graphite oscillator at room (298 K) and low (3 K) temperatures, respectively, with $\gamma/2\pi = 0.13$ Hz. The blue and black dotted curve represents the acceleration sensitivity of processed pyrolytic graphite oscillator with laser engraving pattern. The acceleration sensitivity at room temperature can reach 8×10^{-11} g/$\sqrt{\text{Hz}}$ and at low temperature it can reach 8×10^{-12} g/$\sqrt{\text{Hz}}$. It is worth mentioning that the acceleration sensitivity represented by the red star in Fig. 6 is given by Eq. (1), which represents the acceleration sensitivity when the system reaches the thermal noise limitation. Under

practical experimental conditions, due to the imperfection of the vibration isolation system, the acceleration sensitivity of our experimental system would be slightly worse than this theoretical value.

V. SUMMARY AND DISCUSSION

We propose an engineering conductive geometry scheme for diamagnetically levitated millimeter pyrolytic graphite oscillator, which can prevent the formation of eddy currents, so as to shift the dissipation from eddy current dominance to pressure dominance. Our experiments demonstrate that the use of the processed diamagnetically levitated pyrolytic graphite oscillator with 50 slits suppresses the mechanical dissipation by 50 times compared to the unprocessed ones, under high vacuum at room temperature. To improve the acceleration sensitivity of the oscillator, we need to reduce the ratio γ/m. For the pyrolytic graphite oscillator in this experiment, the acceleration sensitivity is gradually improved with the increase of the mass. When the mass of the oscillator reaches 200 mg, it can reach 10^{-11}g/$\sqrt{\text{Hz}}$ at room temperature. Our method is an effective way to increase the acceleration sensitivity of the oscillator while maintaining the oscillator's levitation capability.

The engineering conductive geometry scheme reported here has potential for further improvements. Due to the limitation of laser engraving technology and vacuum condition, this scheme has not been realized at its theoretically best value. At present, the minimum slit width that our technology can achieve is 0.04 mm. With more and denser slits, the eddy current dissipation of the oscillator can be further reduced. Furthermore, the passive levitation system in our experiment has no additional source of noise, it is appropriate for low-temperature environments, which have lower thermal noise levels. In future work, We hope to transplant our system to a cryogenic platform, and the system can be pumped into a higher vacuum. As a result, the acceleration detection sensitivity can be improved by at least one order of magnitude. It would be a huge potential advantage in the field of precision measurement [41–43], in spite of more strict requirements for the vibration isolation system. This work opens a new door for studying fundamental physical models by laboratory experiment in the future, such as wave-function collapse models [44–46] and dark energy [47].

Recently, we have noticed that a similar method is used in pyrolytic graphite oscillators to reduce the mechanical dissipation from eddy current damping [48,49].
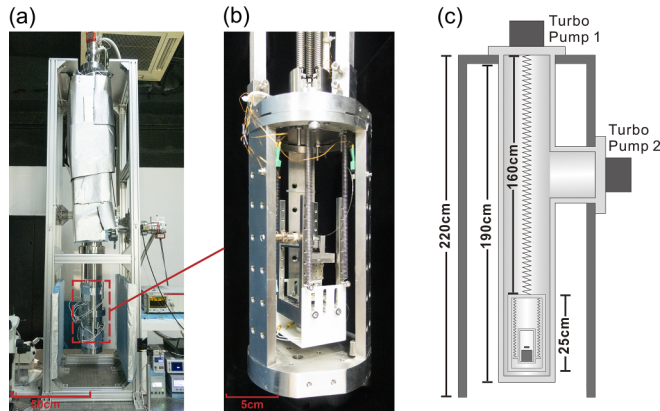
FIG. 7. Vibration isolation system. (a) The overall appearance of the experimental system. (b) The two-stage vibration isolation system in the vacuum chamber. The primary vibration isolation platform with a mass of 8.2 kg is suspended by the springs. The secondary vibration isolation platform is suspended on the primary vibration isolation platform by springs and equipped with trap, fibers and so on, with a total mass of 0.8 kg. (c) Sketch of the vibration isolation system. The height of the external frame is 220 cm, the overall length of the vacuum chamber is 190 cm. The length of the primary vibration isolation spring is 160 cm, the length of the cylinder is 25 cm, and the length of the secondary vibration isolation spring is 16 cm. We used two turbo pumps to achieve a stable vacuum in our system.

APPENDIX: VIBRATION ISOLATION SYSTEM

As shown in Figs. 7(a) and 7(b), our experiment system is fixed on a 2.2 m aluminum frame, and there is a two-stage vibration isolation system inside the vacuum chamber. We used springs to suspend the primary and secondary vibration isolation platforms, the mass of the vibration isolation platform is 8.2 and 0.8 kg, respectively. Figure 7(c) is the sketch of the vibration isolation system.

We test our vibration isolation system by measuring the power spectrum density (PSD) of voltage S_V at different pressures. As shown in Figs. 8(a) and 8(b), at the pressure of 5.1×10^{-3} mbar, the $\gamma/2\pi$ of pyrolytic graphite oscillator in z-mode motion is 0.012 Hz, and the integral area of S_V is 6.9 ± 0.4 mV^2. At the pressure of 1.4×10^{-4} mbar, the $\gamma/2\pi$
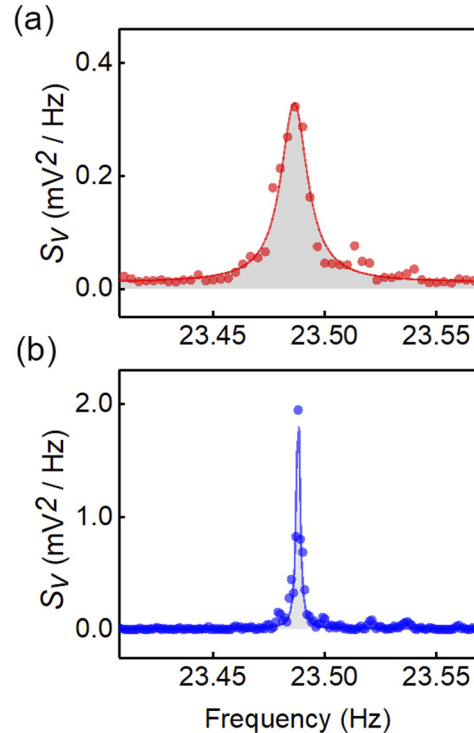

FIG. 8. Power spectral density (PSD) S_V of the pyrolytic graphite oscillator in z-mode at different pressures. (a) At the pressure of 5.1×10^{-3} mbar, the $\gamma/2\pi$ of oscillator is 0.012 Hz, and the integral area of S_V (gray shadow area) is 6.9 ± 0.4 mV^2. (b) At the pressure of 1.4×10^{-4} mbar, the $\gamma/2\pi$ is 0.002 Hz and the integral area of S_V is 8 ± 0.6 mV^2. In high vacuum, the impact of environmental vibration on our system is about 20% of the thermal motion.

is 0.002 Hz and the integral area of S_V is 8 ± 0.6 mV^2. The impact of environmental vibrations on our system is about 20% of the thermal motion in high vacuum, and the oscillator is nearly in thermal equilibrium. The possible source of noise is the wires of fiber and thermometer connected to the vibration isolation system. It is worth mentioning that we measured the free decaying curve and mechanical dissipation by exciting the oscillator using an excitation coil. In this procedure, the oscillator's excitation amplitude is much larger than thermal motion.

[1] D. E. Chang, C. A. Regal, S. B. Papp, D. J. Wilson, J. Ye, O. Painter, H. J. Kimble, and P. Zoller, Cavity opto-mechanics using an optically levitated nanosphere, Proc. Natl. Acad. Sci. USA **107**, 1005 (2010).

[2] Y. Leng, R. Li, X. Kong, H. Xie, D. Zheng, P. Yin, F. Xiong, T. Wu, C.-K. Duan, Y. Du, Zhang-qi Yin, P. Huang, and J. Du, Mechanical Dissipation Below 1 μHz with a Cryogenic Diamagnetic Levitated Micro-Oscillator, Phys. Rev. Appl. **15**, 024061 (2021).

[3] V. B. Braginsky, V. P. Mitrofanov, and V. I. Panov, *Systems with Small Dissipation* (University of Chicago Press, Chicago, 1985).

[4] Y. Chen, Macroscopic quantum mechanics: Theory and experimental concepts of optomechanics, J. Phys. B **46**, 104001 (2013).

[5] C. Timberlake, G. Gasbarri, A. Vinante, A. Setter, and H. Ulbricht, Acceleration sensing with magnetically levitated oscillators above a superconductor, Appl. Phys. Lett. **115**, 224101 (2019).

[6] A. Vinante, P. Falferi, G. Gasbarri, A. Setter, C. Timberlake, and H. Ulbricht, Ultralow Mechanical Damping with Meissner-Levitated Ferromagnetic Microparticles, Phys. Rev. Appl. **13**, 064027 (2020).

[7] F. Monteiro, S. Ghosh, A. G. Fine, and D. C. Moore, Optical levitation of 10-ng spheres with nano- g acceleration sensitivity, Phys. Rev. A **96**, 063841 (2017).

[8] C. W. Lewandowski, T. D. Knowles, Z. B. Etienne, and B. D'Urso, High Sensitivity Accelerometry with a Feedback-Cooled Magnetically Levitated Microsphere, Phys. Rev. Appl. **15**, 014050 (2021).

[9] T. Wang, S. Lourette, S. R. O'Kelley, M. Kayci, Y. B. Band, D. F. Jackson Kimball, A. O. Sushkov, and D. Budker, Dynamics of a Ferromagnetic Particle Levitated Over a Superconductor, Phys. Rev. Appl. **11**, 044041 (2019).

[10] J. Gieseler, A. Kabcenell, E. Rosenfeld, J. D. Schaefer, A. Safira, M. J. A. Schuetz, C. Gonzalez-Ballestero, C. C. Rusconi, O. Romero-Isart, and M. D. Lukin, Single-Spin Magnetomechanics with Levitated Micromagnets, Phys. Rev. Lett. **124**, 163604 (2020).

[11] T. Delord, P. Huillery, L. Nicolas, and G. Hétet, Spin-cooling of the motion of a trapped diamond, Nature (London) **580**, 56 (2020).

[12] G. P. Conangla, A. W. Schell, R. A. Rica, and R. Quidant, Motion control and optical interrogation of a levitating single nitrogen vacancy in vacuum, Nano Lett. **18**, 3956 (2018).

[13] A. Vinante, C. Timberlake, D. Budker, D. F. Jackson Kimball, A. O. Sushkov, and H. Ulbricht, Surpassing the Energy Resolution Limit with Ferromagnetic Torque Sensors, Phys. Rev. Lett. **127**, 070801 (2021).

[14] J. Millen, T. Deesuwan, P. Barker, and J. Anders, Nanoscale temperature measurements using non-equilibrium Brownian dynamics of a levitated nanosphere, Nat. Nanotechnol. **9**, 425 (2014).

[15] E. Hebestreit, R. Reimann, M. Frimmer, and L. Novotny, Measuring the internal temperature of a levitated nanoparticle in high vacuum, Phys. Rev. A **97**, 043803 (2018).

[16] D. F. Jackson Kimball, A. O. Sushkov, and D. Budker, Precessing Ferromagnetic Needle Magnetometer, Phys. Rev. Lett. **116**, 190801 (2016).

[17] J.-F. Hsu, Peng Ji, C. W. Lewandowski, and B. D'Urso, Cooling the motion of diamond nanocrystals in a magneto-gravitational trap in high vacuum, Sci. Rep. **6**, 30125 (2016).

[18] A. Vinante, G. Gasbarri, C. Timberlake, M. Toroš, and H. Ulbricht, Testing dissipative collapse models with a levitated micromagnet, Phys. Rev. Res. **2**, 043229 (2020).

[19] A. Pontin, N. P. Bullier, M. Toroš, and P. F. Barker, Ultranarrow-linewidth levitated nano-oscillator for testing dissipative wave-function collapse, Phys. Rev. Res. **2**, 023349 (2020).

[20] G. Gasbarri, A. Belenchia, M. Carlesso, S. Donadi, A. Bassi, R. Kaltenbaek, M. Paternostro, H. Ulbricht, Testing the foundations of quantum physics in space Interferometric and non-interferometric tests with large particles, Commun. Phys. **4**, 155 (2021).

[21] A. Vinante and H. Ulbricht, Gravity-related collapse of the wave function and spontaneous heating: Revisiting the experimental bounds, AVS Quantum Sci. **3**, 045602 (2021).

[22] D. S. Ether, L. B. Pires, S. Umrath, D. Martinez, Y. Ayala, B. Pontes, G. R. de S. Araújo, S. Frases, G. L. Ingold, F. S. S. Rosa, N. B. Viana, H. M. Nussenzveig, and P. A. Maia Neto, Probing the Casimir force with optical tweezers, Europhys. Lett. **112**, 44001 (2015).

[23] A. A. Geraci, S. B. Papp, and J. Kitching, Short-Range Force Detection Using Optically Cooled Levitated Microspheres, Phys. Rev. Lett. **105**, 101101 (2010).

[24] G. Winstone, R. Bennett, M. Rademacher, M. Rashid, S. Buhmann, and H. Ulbricht, Direct measurement of the electrostatic image force of a levitated charged nanoparticle close to a surface, Phys. Rev. A **98**, 053831 (2018).

[25] A. Arvanitaki and A. A. Geraci, Detecting High-Frequency Gravitational Waves with Optically Levitated Sensors, Phys. Rev. Lett. **110**, 071105 (2013).

[26] N. Aggarwal, G. P. Winstone, M. Teo, M. Baryakhtar, S. L. Larson, V. Kalogera, and A. A. Geraci, Searching for New Physics with a Levitated-Sensor-Based Gravitational-Wave Detector, Phys. Rev. Lett. **128**, 111101 (2022).

[27] G. Winstone, Z. Wang, S. Klomp, G. R. Felsted, A. Laeuger, C. Gupta, D. Grass, N. Aggarwal, J. Sprague, P. J. Pauzauskie, S. L. Larson, V. Kalogera, and A. A. Geraci (LSD Collaboration), Optical Trapping of High-Aspect-Ratio NaYF Hexagonal Prisms for kHz-MHz Gravitational Wave Detectors, Phys. Rev. Lett. **129**, 053604 (2022).

[28] D. C. Moore, A. D. Rider, and G. Gratta, Search for Millicharged Particles Using Optically Levitated Microspheres, Phys. Rev. Lett. **113**, 251801 (2014).

[29] A. D. Rider, D. C. Moore, C. P. Blakemore, M. Louis, M. Lu, and G. Gratta, Search for Screened Interactions Associated with Dark Energy below the 100 μm Length Scale, Phys. Rev. Lett. **117**, 101101 (2016).

[30] A. Kawasaki, Search for kilogram-scale dark matter with precision displacement sensors, Phys. Rev. D **99**, 023005 (2019).

[31] F. Monteiro, G. Afek, D. Carney, G. Krnjaic, J. Wang, and D. C. Moore, Search for Composite Dark Matter with Optically Levitated Sensors, Phys. Rev. Lett. **125**, 181102 (2020).

[32] D. Carney, S. Ghosh, G. Krnjaic, and J. M. Taylor, Proposal for gravitational direct detection of dark matter, Phys. Rev. D **102**, 072003 (2020).

[33] D. Budker, T. Cecil, T. E. Chupp, A. A. Geraci, D. F. Jackson Kimball, S. Kolkowitz, S. Rajendran, J. T. Singh, and A. O. Sushkov, Quantum sensors for high precision measurements of spin-dependent interactions, arXiv:2203.09488.

[34] D. Carney, Y. Chen, A. Geraci, H. Müller, C. D. Panda, P. C. E. Stamp, J. M. Taylor, Snowmass 2021 White Paper: Tabletop experiments for infrared quantum gravity, arXiv:2203.11846.

[35] P. Fadeev, C. Timberlake, T. Wang, A. Vinante, Y. B. Band, D. Budker, A. O. Sushkov, H. Ulbricht, and D. F. Jackson Kimball, Ferromagnetic gyroscopes for tests of fundamental physics, Quantum Sci. Technol. **6**, 024006 (2021).

[36] J. S. Pedernales, K. Streltsov, and M. B. Plenio, Enhancing Gravitational Interaction between Quantum Systems by a Massive Mediator, Phys. Rev. Lett. **128**, 110401 (2022).

[37] Y. Michimura and K. Komori, Quantum sensing with milligram scale optomechanical systems, Eur. Phys. J. D **74**, 126 (2020).

[38] K. Streltsov, J. S. Pedernales, and M. B. Plenio, Ground-State Cooling of Levitated Magnets in Low-Frequency Traps, Phys. Rev. Lett. **126**, 193602 (2021).

[39] C. A. Klein, Electrical properties of pyrolytic graphite, Rev. Mod. Phys. **34**, 56 (1962).

[40] F. Xiong, P. Yin, T. Wu, H. Xie, R. Li, Y. Leng, Y. Li, C. Duan, X. Kong, P. Huang, and J. Du, Lens-Free Optical Detection of Thermal Motion of a Submillimeter Sphere Diamagnetically Levitated in High Vacuum, Phys. Rev. Appl. **16**, L011003 (2021).

[41] J. Gieseler, L. Novotny, and R. Quidant, Thermal nonlinearities in a nanomechanical oscillator, Nat. Phys. **9**, 806 (2013).

[42] G. Ranjit, M. Cunningham, K. Casey, and A. A. Geraci, Zeptonewton force sensing with nanospheres in an optical lattice, Phys. Rev. A **93**, 053801 (2016).

[43] D. Hempston, J. Vovrosh, M. Toroš, G. Winstone, M. Rashid, and H. Ulbricht, Force sensing with an optically levitated charged nanoparticle, Appl. Phys. Lett. **111**, 133111 (2017).

[44] D. Zheng, Y. Leng, X. Kong, R. Li, Z. Wang, X. Luo, J. Zhao, C.-K. Duan, P. Huang, J. Du, M. Carlesso, and A. Bassi, Room temperature test of the continuous spontaneous localization model using a levitated micro-oscillator, Phys. Rev. Res. **2**, 013057 (2020).

[45] L. Diósi, Testing Spontaneous Wave-Function Collapse Models on Classical Mechanical Oscillators, Phys. Rev. Lett. **114**, 050403 (2015).

[46] J. Li, S. Zippilli, J. Zhang, and D. Vitali, Discriminating the effects of collapse models from environmental diffusion with levitated nanospheres, Phys. Rev. A **93**, 050102(R) (2016).

[47] J. Khoury and A. Weltman, Chameleon cosmology, Phys. Rev. D **69**, 044026 (2004).

[48] X. Chen, S. K. Ammu, K. Masania, P. G. Steeneken, and F. Alijan, Diamagnetic composites for high-Q levitating resonators, Adv. Sci. **9**, 2203619 (2022).

[49] P. Romagnoli, R. Lecamwasam, S. Tian, J. Downes, and J. Twamley, Controlling the motional quality factor of a diamagnetically levitated graphite plate, arXiv:2211.08764.